https://doi.org/10.33805/2572-6978.106
Volume 2 • Issue 1 | P: 106 | Page 1 of 11

EDELWEISS PUBLICATIONS
OPEN ACCESS

Dental Research and Management

Research Article ISSN: 2572-6978

Observations of Enamel Microstructure in Incipient Lesions Remineralized by NaF Dentifrices

Makoto Asaizumi[1]*, Naoto Yagi[2], Koki Aoyama[2], Tomoaki Kato[3], Tetsuya Kuga[3], Nahoko Oode[4], Takehide Oda[4], Tsuguo Sakurada[4], Shinichi Nagase[5], Tomohiro Tabara[6] and Robert L. Karlinsey[7]

Abstract

Synchrotron Radiation (SR) Wide-angle X-ray Diffraction (WAXD) and Small-angle X-ray Scattering (SAXS) techniques were used to assess microstructure of bovine enamel white-spot lesions (WSL) evaluated in a 10-day pH cycling model comprising three different dentifrice groups: (A) 0.21% NaF plus TCP (Clinpro Tooth Crème), (B) 1.1% NaF plus TCP (Clinpro 5000), or (C) 0% NaF (Tom's of Maine) dentifrice. Each day consisted of four 2-minute treatments, one 4-hour acid challenge (pH=5.0), and immersion in artificial saliva (pH=7.0) between these events. These specimens were also examined with cross-sectional microhardness, digital light microscopy and FE-SEM (field emission scanning electron microscope), and demonstrated the remineralization model effected changes in subsurface microstructure. X-ray diffraction data from WAXD and SAXS were collected on enamel slab cross-sections extending from 0 μm to 150 μm, in 6 μm microbeam increments. A primary outcome of this observational study was that simultaneous WAXD and SAXS measurements were able to resolve significant differences (ANOVA, Student's t-test, $p<0.05$) between the effects of the two fluoride-containing dentifrices on subsurface lesion microstructure. In particular, enamel lesions treated with 1.1% NaF dentifrice group manifested an abundance of nanometer-sized crystallites, while treatment with the 0.21% NaF dentifrice produced larger apatite-like crystals. While the presence of fluoride in both cases promoted regularity in crystal size and orientation, this was not observed for lesions treated without fluoride. Altogether, our observations demonstrate the pathological processes for remineralization are markedly influenced by the presence and concentration of fluoride, the microstructural characteristics of which can be distinguished using the simultaneous WAXD and SAXS technique.

Keywords: Synchrotron Radiation; WAXD; SAXS; Remineralization; Fluoride; Calcium and Phosphate; Subsurface Lesion; Enamel

Introduction

Dental researchers and clinicians have long recognized the viability of reducing dental caries with fluoride [1]. But the multifactorial nature of tooth decay contributes to the still problematic issue of tooth decay and therefore continues to command attention, which includes improved understanding of not only the effect of caries on the tooth but also the effect of preventive agents on the carious tooth, including topical fluorides [2,3].

Carious lesions manifest a subsurface environment devoid of mineral [4], the nature of which are now routinely studied using a variety of methodologies, including micro hardness techniques, optical or electronic microscopies, and transverse X-ray microradiography [5,6]. Investigations of enamel micro- and ultrastructure, such as identification of particular mineral phases or characteristics of crystalline framework, wide-angle X-ray diffraction (WAXD), small-angle X-ray scattering (SAXS), conventional or synchrotron radiation-based micro-computed tomography, and electron microscopies are typically used [7-15]. Among these techniques, scanning or transmission electron microscopies have been used with much success for over 30 years to reveal intricacies of enamel ultrastructure, including the identification of defects manifest in dental apatite (e.g. point defects, edge defects, screw dislocations, and small angle boundary defects) [14-18].

With recent technical advancements in X-ray apparatus (e.g. narrowing of X-ray beam width), SAXS experiments have revealed new information [7,8,10]. Recently, a SAXS investigation revealed the underlying nanoscale enamel crystalline framework

Affiliation:

[1]*Dr. Makoto Asaizumi Orthodontic Practice, Ban Bldg. 3F, 1-8 Chiyodacho, Mobara, Chiba 297-0023, Japan*

[2]*SPring-8 / JASRI, 1-1-1 Kouto, Sayocho, Sayogun, Hyogo 679-5198, Japan*

[3]*Dr. Tetsuya Kuga Dental Practice, 924 Kamiichiba, Mutsuzawamachi, Chouseigun, Chiba 299-4403, Japan*

[4]*JFE Techno-Research Corporation, 1-1 Minami Wataridacho, Kawasakiku, Kawasaki, Kanagawa 210-0855, Japan*

[5]*Ozsystem Ltd., 1-5-23 Oohasuhigashi, Higashiosaka, Osaka 577-0824, Japan*

[6]*Carl Zeiss Microscopy Japan Co., Ltd., 7 Honshiocho, Shinjukuku, Tokyo 160-0003, Japan*

[7]*Indiana Nanotech, 14 East Washington Street, Suite 6A, Indianapolis, IN 46204, USA*

***Corresponding author:**
Makoto Asaizumi, Dr. Makoto Asaizumi Orthodontic Practice, Ban Bldg. 3F,1-8 Chiyodacho, Mobara, Chiba 297-0023, Japan,
Tel: +81-475-27-1901; Fax: +81-475-27-1902
E-mail: asaizumi.ortho.praxis@gmail.com

Citation: Asaizumi M, Yagi N, Aoyama K, Kato T, Kuga T, et al. (2017) Observations of Enamel Microstructure in Incipient Lesions Remineralized by NaF Dentifrices. Dent Res Mang. 2: 20-30

Received: Nov 02, 2016
Accepted: Feb 02, 2017
Published: Feb 06, 2017

retains anisotropy in both incipient and advanced carious lesions [10]. Separately, quantitative detection of inter-crystalline voids in demineralized enamel has been achieved using SAXS [7,8]; in doing so, these SAXS studies demonstrated the crystallite-void relationship within carious enamel microstructure is sensitive to remineralization [8].

In our previous work, we have probed the microstructure of incipient enamel lesions cycled in a 10-day *in vitro* remineralization model using a conventional and synchrotron radiation micro-computed tomography [12,13]. *In vitro* cycling models manifest evens corresponding to treatment, acid challenge or salivary events, and are useful in assessing the quality of newly formed mineral [5]. The remineralization model employed in this study is sensitive to fluoride and has been used successfully to correlate with clinical outcomes [5,6,19-23]. The outcome of those pilot studies revealed synchrotron radiation micro-computed tomography could resolve significant microstructural differences in incipient lesions subjected to three different dentifrices, including a fluoride-free dentifrice (Tom's of Maine) along with 0.21% NaF and 1.1% NaF dentifrices (3M Clinpro Tooth Crème and Clinpro 5000, respectively). Those encouraging results prompted us to continue our microstructural investigations into the remineralized carious lesions.

In the present investigation we have used a plurality of techniques to probe the enamel microstructure of the same incipient carious lesions previously evaluated with micro-computed tomography. In particular, we utilized the BL40XU beamline of the SPring-8 third-generation synchrotron radiation facility in Hyogo, Japan to collect WAXD and SAXS measurements within the incipient lesions. This advanced facility provided us an opportunity to evaluate the microstructural environment of incipient lesions subject to topical fluoride treatments in an *in vitro* remineralization model. Additionally, digital light microscopy, high-resolution field-emission scanning electron microscopy (FE-SEM) and microhardness measurements were also employed to investigate the effect of the three different dentifrice treatments on subsurface morphology and strength.

Experimental Section

Treatment groups and pH-cycling study

As this study is a follow-on to the previous laboratory study and utilized the same enamel specimens as used previously, in-depth experimental details on specimens preparation, demineralization and remineralization solutions, and white-spot lesion formation can be found in greater detail in our prior publications [12,13]. The same bovine enamel specimens (N=20 per group) as examined previously were maintained in their respective groups as follows:

(A) 0.21% NaF plus TCP (Clinpro Tooth Crème, 3M, USA); and,

(B) 1.1% NaF plus TCP (Clinpro 5000, 3M, USA); and,

(C) 0% NaF (Tom's of Maine, Colgate, USA).

Each group of enamel specimens were cycled in a remineralization/demineralization pH cycling model lasting 10 days [6,12,19,21]. This daily cycling model comprised immersion of inverted specimens in two two-minute treatment events performed an hour apart in the morning, followed by one four-hour polyacrylic acid-lactic acid challenge (15 mL, pH=5.0), and finally two more two-minute treatment events in the afternoon. Treatments were diluted with distilled water (5g paste: 10 ml distilled water). Specimens were inverted and immersed in artificial saliva in between the daily treatments and acid challenge, as well as overnight. An example of 10 enamel specimens mounted in acrylic and cycled in this pH model is shown in Figure 1.

Cross-sectional microhardness (CSMH)

Ten of the 20 cycled specimens from each dentifrice group, along with 10 sound and 10 WSL enamel specimens, were then prepared for CMSH assessments. First, a Lapcraft Lil'Trimmer circular saw (Powell, OH, USA) was used to section the enamel specimens. The sections were then mounted with ClaroCit methylmethacrylate-based cold mounting resin (Struers, Cleveland, OH, USA) with the freshly cut surfaces exposed. The mounted specimens were serially ground with 100, 600 and 1000 grit sandpaper (3M, St. Paul, MN, USA), and then serially polished using a Leco Spectrum System 1000 grinder/polisher with 3 μm microid diamond compound and compound extender for lubricant. Due to the delicacy of the enamel in the white-spot lesion zone, which can lead to undesirable cracking upon indentation, along with the spatial limitations of multiple indents, we selected the Knoop indenter over the Vickers indenter. A series of three indentation lanes per specimen were made under a load of 10 gf at 12.5 μm, 25 gf at 25 and 37.5 μm, and 50 gf at 50, 75 and 100, 125 and 150 μm below the specimen surface. Measurements closer to the enamel surface (i.e. less than 12.5 μm was not feasible at the given load limits due to the delicacy of the specimens. This resulted in a total of 24 indents per specimen. The Knoop indentation lengths were then converted to Knoop Hardness Numbers (KHN). Relative to the KHN of sound enamel, relative lesions sizes in units of square root of KHN (√KHN) multiplied by enamel depth (i.e. from 12.5 to 150 μm) were calculated using Simpson's Composite Rule [24,25]. In doing so, this estimated lesion size (which is an area, with units of √KHN*μm) can be correlated with approximate mineral volume content determined by transverse microradiography.

Figure 1: Top-view photograph of bovine enamel specimens mounted in acrylic and subjected to the pH cycling model.

Sample preparation for digital light microscopy, FE-SEM and WAXD/SAXS measurements

The remaining 10 (of the 20) specimens cycled in the pH model discussed above were then prepared for light microscopy, FE-SEM and X-ray experiments. Thin enamel slices were excised from the specimens cycled in the pH model; additionally, a separate set of 10 sound and 10 WSL specimen slices were also excised. Excision was performed using KaVo Gentlesilence LUX 800B handpiece with diamond point HP25B (Shofu Co. Japan). After grinding and polishing with waterproof abrasive paper (type DCC 400, 800 and 2000 grit, Sankyo Rikagaku Co. LTD., Japan) by hand, the excised enamel slabs had approximate thickness of 100 μm. While there exists the possibility that enamel structure could be altered during the polishing procedure, we note the relatively high inter-crystalline density of the enamel specimens helps reduce the risk for alteration of crystal morphology [14,15,18]. Notably, similar polishing procedures in preparation of enamel cross-sections for microhardness and optical measurements are routinely used but have not demonstrated evidence of morphological alteration [5-8,14,24,25]; thus, based on our polishing technique, along with assessments made at different positions of multiple specimens (notably for the WAXD and SAXS measurements), we believe the risk for introducing morphological anomalies via polishing is relatively low.

Digital light microscopy

Thin enamel slices were randomly selected and assessed for thickness and lesion depth with an Axio Imager 2 digital light microscope (Zeiss Corporation, Germany). Darkfield reflected light was used to confirm slice thickness using a Neofluar lenz objective at 50x magnification. Brightfield reflected light was used to assess lesion depth of the enamel slice cross-sections using an Apochromat lenz objective at 200x magnification.

Field emission scanning electron microscopy (FE-SEM)

The thin enamel slices were randomly selected for evaluation with a Zeiss Ultra 55 ultra-low voltage field-emission scanning electron microscope (Germany). Samples were treated with osmium tetroxide (Neoc-STB, Meiwaforsis Co., Japan) to reduce electrical charging of samples. SE2 (Out-Lens SE (secondary-electron image) detector) and In-Lens SE detectors were used to collect scattered electrons operating at 1 kV. The aperture was fixed at 60 μm and high-resolution magnifications of 2,000x (for the SE2 detector) and 30,000x (for the In-Lens SE detectors were used to image enamel slice cross-sections from each of the five groups.

Wide-angle X-ray diffraction (WAXD) and small-angle X-ray scattering (SAXS) Measurements

X-ray diffraction experiments were performed at BL40XU of SPring-8 synchrotron radiation facility (Hyogo, Japan) with X-ray energy of 15.0 keV [26]. A schematic of the experimental setup is shown in Figure 2, and both SAXS (equatorial scattering) and WAXD ((100) reflection) were measured with the same detector [7,8]. An X-ray microbeam was obtained by placing a 5 μm collimating pinhole on the focused beam [27]. The beam was expanded to about 6 μm at the sample due to Fresnel diffraction. A guard pinhole with a diameter of 200 μm was placed in front of the sample, resulting in an 80 mm separation between the two pinholes. The X-ray flux was about 3×10^{11} photons/sec, and the X-ray detector was X-ray image intensifier (V7739, Hamamatsu Photonics, Hamamatsu, Japan) coupled with a tandem lens to a cooled CCD camera (ORCA-II-ER, Hamamatsu Photonics). The reciprocal spacing was calibrated with a powder diffraction pattern of behenic acid silver salt (silver behenate). Enamel slabs were then mounted vertically [Figure 3]. The X-ray beam passed perpendicularly through each enamel slab surface. For each enamel slab, the sample was moved to the left from the monitor's view [Figure 4] so that the X-ray beam scanned across the enamel from the surface towards dentin in 6 μm steps. Diffraction patterns were recorded beginning in the airspace above the horizontal slab surface down to 260 μm (only for those treated with Clinpro 5000 due to sample limitations) or 300 μm (all other groups); however, the ROI (region of interest) in our study spanned from the edge of the slab surface down to 200 μm, and included the sound and demineralized enamel zones only, so the difference between 260 μm and 300 μm is a non-factor in our assessment of enamel structure. For each enamel slab, 10 scans along different regions (i.e. height of slab was adjusted) of the sample were collected in order to generate a mean profile for the given sample. The detector

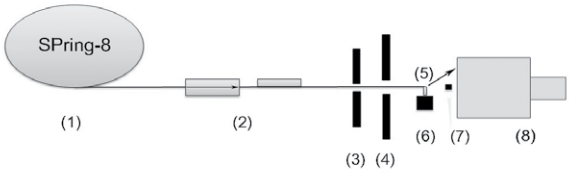

Figure 2: Schematic diagrams of the X-ray diffraction measurement set-up at BL40XU in the SPring-8 synchrotron radiation facility. The numbers indicate the following items: (1) synchrotron X-ray source (SPring-8), (2) two focusing mirrors, (3) collimating pinhole (about 5 μm diameter), (4) guard pinhole (200 μm diameter), (5) specimen (thin slice of bovine enamel), (6) remote-controlled vertical translation stage, (7) beam stop to avoid exposure of the direct beam on the detector, (8) X-ray detector (an image intensifier combined with a cooled CCD camera), Approximate distances are: from (1) to (2): 40 m; from (2) to (3): 10 m; from (3) to (4): 80 mm; from (4) to (5): 10 mm. The distance from (5) to (7) was about 200 mm.

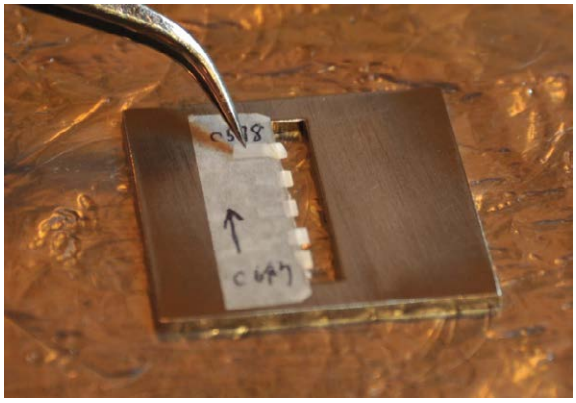

Figure 3: An example photograph of five thin enamel slabs mounted on a metal sample holder. All slabs were aligned within the window with the enamel edge made as horizontal as possible for the impinging perpendicular X-ray beam.

exposure time was 600 msec. A representative photograph of the relative sample and detector positions is shown in Figure 5. We note that this simultaneous WAXD/SAXS experimental setup reduces the scatter arc impinging on the detector, and results in the lack of the characteristic (002) reflection commonly found for enamel.

WAXD and SAXS Analyses

Fit2D software version 012 077 i686 WXP (ESRF98HA01T, France) was used to determine intensity collected from each enamel specimen at each depth. VB program (Ozsystem, Japan) was made accommodate the 24,500 CHI files of WAXD and SAXS data. WAXD/SAXS data ranging from 0 μm to 150.0 μm, with 6.0 μm increments were analysed. Data points lying outside of ±2 SD were considered outliers. Additional analytical detail can be found in a prior publication [7].

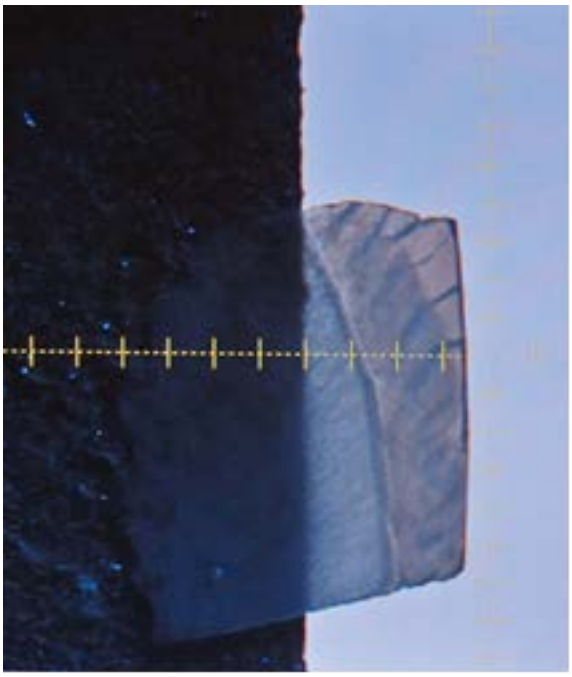

Figure 4: Example monitor view of the mounted enamel slab (thickness ~ 100 μm) from the Experimental Hutch. Each sample was scanned from the right (outer enamel surface) to the left (towards dentin) at 10 different slab positions using a remote-controlled vertical translation stage. The ROI (region of interest) spanned the edge of the slab down to 200 μm.

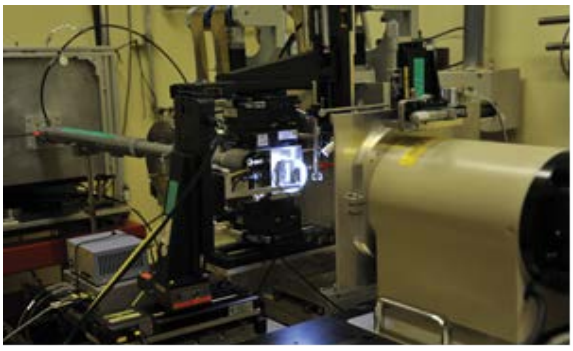

Figure 5: Photographic view of the stage (illuminated) and X-ray detector (far right). The enamel slabs were mounted on a windowed metal plate. The position of each slab was adjusted using a remote-controlled vertical translation stage to select the ROI and recorded using the X-ray detector and camera.

Statistical Analyses for CSMH and WAXD/SAXS data

Based on our prior work, there was a desire to probe whether significant differences between the two Clinpro dentifrices could be identified in the CSMH and WAXD/SAXS data sets; thus, statistical analyses were only performed comparing these two groups (A and B) in order to draw parallels to our previous studies. In doing so, a full statistical treatment of the data collected from all the methods used in this study and for all the groups was intentionally not performed as this was not the primary focus of the study. Statistics were determined using the statistical package SAS-JMP (SAS Institute, USA). The mean values of KHN, WAXD and SAXS at each depth (12.5 μm through 150 μm for KHN, 0 μm through 150 μm for WAXD and SAXS) for Clinpro Tooth Crème (A) and Clinpro 5000 (B) were defined as independent variables. Each measurement was considered of equivalent variance so parametric testing (Student's t-test) of the mean value between Clinpro Tooth Crème and Clinpro 5000 was performed. Data points lying outside of 2 SD were considered outliers. Data were normally distributed.

Results

Cross-sectional microhardness (CSMH)

Ten (of the 20) specimens cycled in the pH model were assessed for CSMH. Ten sound and ten WSL control specimens were also evaluated for CSMH. The mean Knoop Hardness Number (KHN) for WSL treated with each of the dentifrices at enamel depths ranging from 12.5 μm to 150 μm is shown in Figure 6. For reference purposes, the depth-dependent KHN values for control sound (S) and WSL (W) are also shown. CSMH measurements on sound enamel yields a relatively constant profile. We note

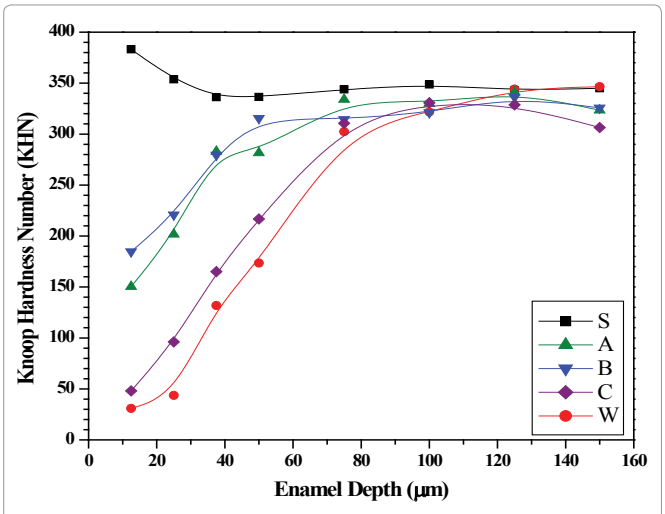

Figure 6: CSMH line profiles for the five groups (**A**, **B**, **C**, **S** and **W**) assessed for Knoop Hardness along the enamel cross-sections. Estimated lesion sizes for groups **A**, **B**, **C** and **W** were made using these CSMH line profiles. The letters correspond to the following groups: 0.21% NaF dentifrice (**A**); 1.1% NaF dentifrice (**B**); 0% NaF dentifrice (**C**); sound enamel control (**S**); and, WSL control (**W**).

that microhardness measurements are recorded by adjusting the applied load to best match the strength of the material of interest. To avoid the risk of fracture near the outer surface of the delicate specimens, lower loads (i.e. 10 gf and 25 gf, respectively) were used in assessing the strength of the WSL specimens (from the three dentifrices groups and the WSL control) at the depths of 12.5 μm and 25 μm. The load of 50 gf was used for all five groups at depths spanning 37.5 μm to 150 μm. The observation of slightly elevated KHN values at 12.5 and 25 μm may be attributed to indentation size effects, which may arise from inherent structural variations within substrates [28], including the differences in strength between enamel near the outer surface and that closer to dentin [29].

The CSMH profile exhibiting the lowest KHN values corresponds to the control WSL (W). CSMH recovery to hardness similar to sound enamel (S) appears about 75 μm for the four WSL groups. All three dentifrice groups produced stronger enamel relative to the baseline WSL control, demonstrating the pH model is sensitive to remineralization. Among the three dentifrice groups, the enamel lesions exposed to the fluoride-free dentifrice (C: Tom's of Maine) produced significantly lower KHN values within the body of the lesion [Figure 6]. The 0.21% NaF (A: Clinpro Tooth Crème) and 1.1% NaF (B: Clinpro 5000) dentifrices were significantly different ($p < 0.05$) only at 50 μm (A < B) and 75 μm (A > B).

The estimated mean (standard error of the mean) relative lesion sizes (in units of √KHN*μm) for the WSL control and the lesions treated with A, B, or C dentifrices in the cycling model were calculated to be 471.4 (35.0), 170.9 (24.5), 191.2 (25.6) and 367.9 (23.7), respectively. The percent remineralization (% Remin) relative to the baseline WSL (W) is expressed as follows:

$$\%Remin = \frac{R_X - D_W}{D_W} \times 100 \quad (1)$$

where D_W corresponds to the WSL control relative lesion size and R_X corresponds to the relative lesion size of W treated with three dentifrices groups (X = A, B or C) in the pH cycling model. Relative to the W control, the % Remin was approximately 64%, 59% and 22%, respectively for each of the dentifrice groups A, B and C. Comparisons in relative lesion size and percent CSMH remineralization between groups A and B were not statistically significant; however, groups A and B were significantly greater than dentifrice group C.

Digital light microscopy

The remaining 10 specimens (from the initial 20) cycled in the pH cycling model were assessed with digital light microscopy to confirm 100 μm slice thicknesses and to view the size of the subsurface lesions after remineralization. Representative darkfield reflected light images of thin enamel slices for each of the five groups (A, B, C, S and W) are shown in Figure 7, where the thickness of the specimen slices was approximately 100 μm. Brightfield reflected light images of the enamel slice cross-sections for each of the five groups (A, B, C, S and W) are shown in Figure 8. The optical lesion size of the control WSL (W) specimen ranges between 60 and 80 μm across the width of the slice. All three dentifrice groups (A, B and C) appear to produce smaller enamel lesions relative to the control WSL, with group B producing the smallest and group C producing the largest.

Field emission scanning electron microscopy (FE-SEM)

Representative FE-SEM images of the five enamel groups at low and high magnifications are compiled in Figures 9 and 10, respectively. Each of the morphologies of the enamel groups are unique and exhibit the following distinctions. The crystallites in sound enamel appear dense and well-ordered (e.g. canted to the right), with most of the widths than 100 nm (approximately). Relative to sound enamel crystallites, the crystallites in WSL enamel appear randomly oriented, loosely-packed and many have estimated widths near to or greater than 100 nm. The crystallites in group A appear to be a combination between sound and WSL

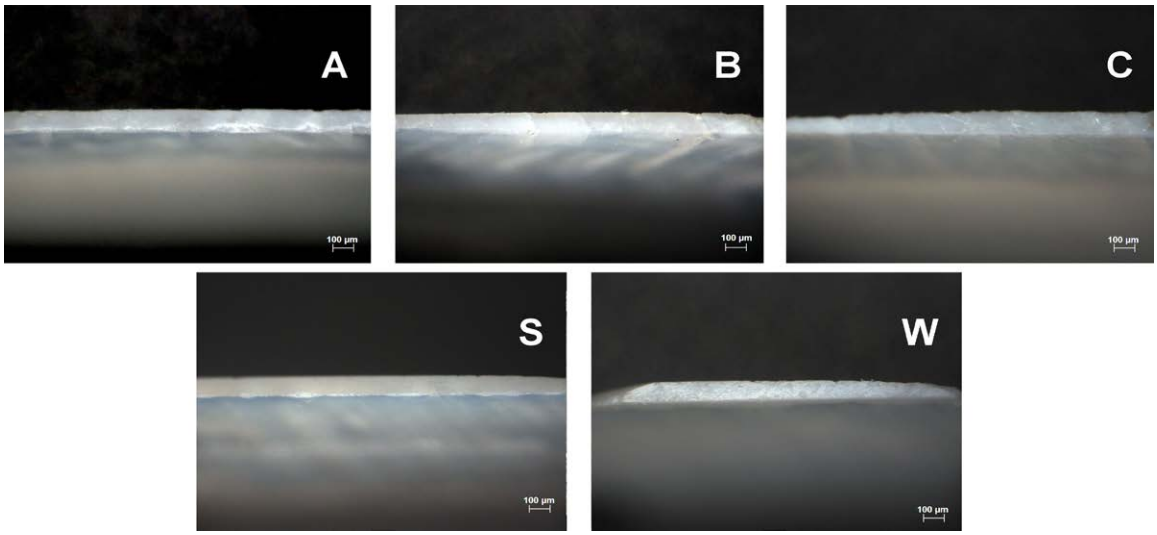

Figure 7: Darkfield reflected light images (Neofluar lenz, 50x magnification, Axio Imager 2, Zeiss Corporation, Germany) of randomly selected enamel slice thickness (about 100 μm) for each of the five groups. The letters correspond to the following groups: 0.21% NaF dentifrice (**A**); 1.1% NaF dentifrice (**B**); 0% NaF dentifrice (**C**); sound enamel control (**S**); and, WSL control (**W**).

enamel crystallites, where the estimated crystallites widths are at or greater than 100 nm but retain, and are relatively dense and well-aligned. The relatively small, densely-packed crystallites in group B differ markedly in morphology and size compared to the other four enamel groups, including the existence of many crystallites smaller than 100 nm. The crystallites in group C are generally larger than 100 nm, are heterogeneously oriented, and are loosely packed, resulting in a relatively porous matrix.

X-ray Diffraction: WAXD and SAXS

Representative WAXD/SAXS patterns from the five groups of enamel specimens (100 μm thick) within the white-spot lesion are shown in Figure 11. Each scattering profile corresponds to the diffraction from hydroxyapatite (HAp) crystallites and is consistent with the patterns obtained previously [7,8]. The principal (100) reflection peak in the sound enamel (S) pattern is indicated with a solid white arrow. Visible in each of the five patterns, this diffraction peak appears prominent for sound enamel but appears attenuated in the WSL control (W) and enamel specimens treated with dentifrices A, B and C. The equatorial scattering (i.e. orthogonal to the *c-axis*) is also present in each of the five patterns and is indicated with a dashed white arrow in the sound enamel pattern.

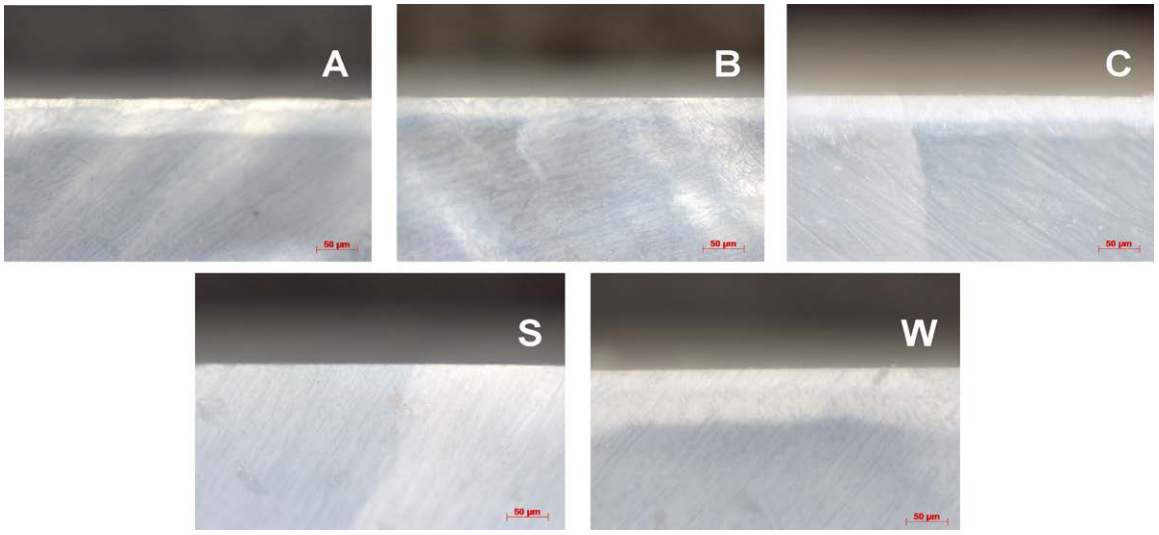

Figure 8: Brightfield reflected light images (Apochromat lenz, 200x magnification, Axio Imager 2, Zeiss Corporation, Germany) of randomly selected enamel slice cross-sections for each of the five groups (the 50 μm scale bar is shown in red on the bottom right). The letters correspond to the following groups: 0.21% NaF dentifrice (**A**); 1.1% NaF dentifrice (**B**); 0% NaF dentifrice (**C**); sound enamel control (**S**); and, WSL control (**W**).

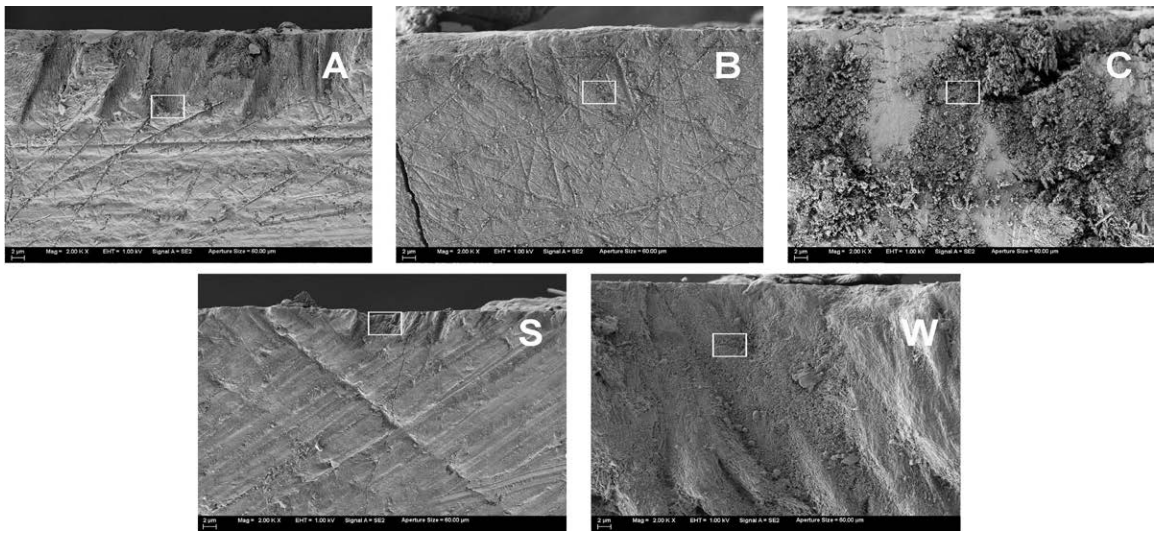

Figure 9: Low magnification (2,000x) FE-SEM images of randomly selected enamel slice cross-sections for each of the five groups under ultra-low voltage conditions (1kV, SE2 detector) at approximately 12 μm into the subsurface lesion. For all images the scale bar corresponds to 2 μm. The white boxes in each image mark the high magnification region for Figure 10. The letters correspond to the following groups: 0.21% NaF dentifrice (**A**); 1.1% NaF dentifrice (**B**); 0% NaF dentifrice (**C**); sound enamel control (**S**); and, WSL control (**W**).

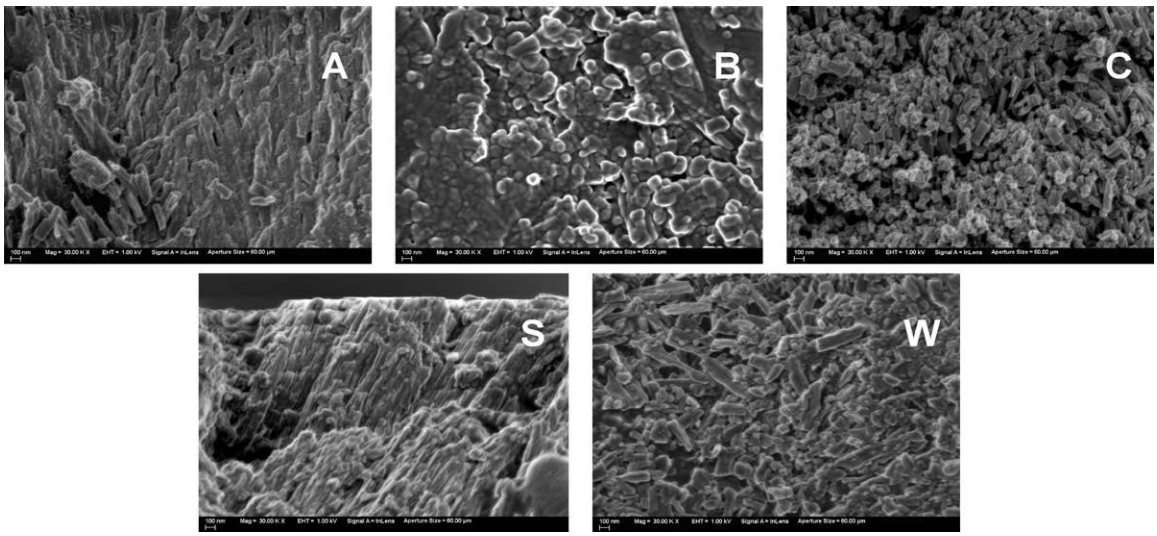

Figure 10: High magnification (30,000x) FE-SEM images of randomly selected enamel slice cross-sections for each of the five groups under ultra-low voltage conditions (1kV, In-Lens SE detector) at approximately 12 μm into the subsurface lesion. For all images the scale bar corresponds to 100 nm. These images pertain to the white square zones shown in Figure 9. The letters correspond to the following groups: 0.21% NaF dentifrice (**A**); 1.1% NaF dentifrice (**B**); 0% NaF dentifrice (**C**); sound enamel control (**S**); and, WSL control (**W**).

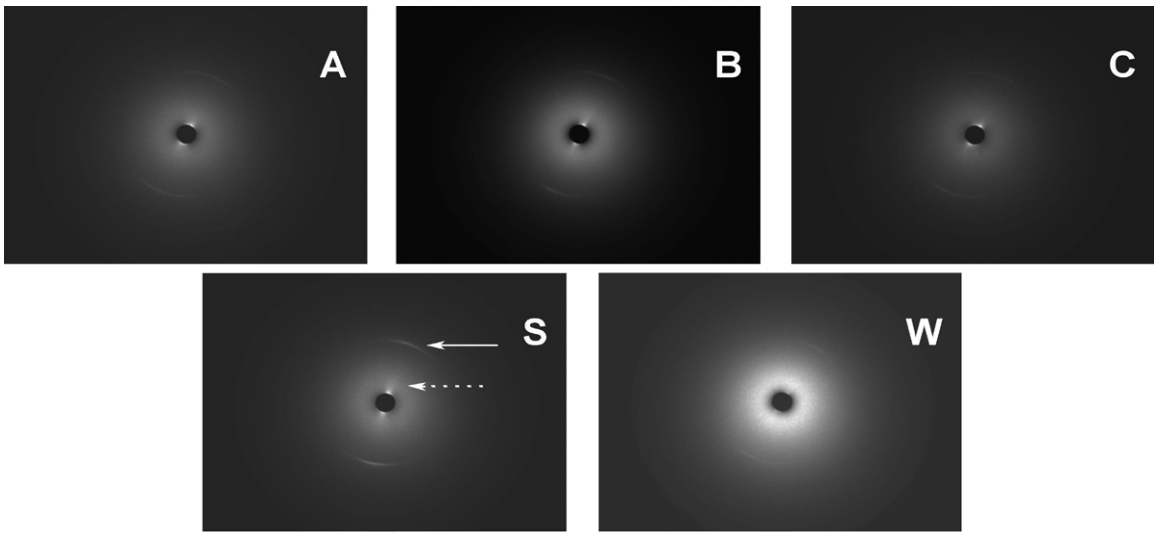

Figure 11: WAXD/SAXS patterns of randomly selected enamel slice cross-sections for each of the five groups at approximately 30 μm into the subsurface lesion. The solid white arrow in S corresponds to the (100) HAp reflection, while the dashed white arrow corresponds to equatorial scattering. The letters correspond to the following groups: 0.21% NaF dentifrice (**A**); 1.1% NaF dentifrice (**B**); 0% NaF dentifrice (**C**); sound enamel control (**S**); and, WSL control (**W**).

The mean normalized integrated intensity of the equatorial (100) HAp reflection from the surface of enamel down to 150 μm in 6 μm increments is shown in Figure 12. For each group, normalization was performed to account for potential variations in enamel slab thickness using the average intensity within the region from 150 to 200 μm. Relative to the sound enamel control, intensity recoveries varied among the groups. The WSL control group produced a unique line profile that gradually recovered beyond 100 μm. Group C specimens produced a different lineshape that recovered around 48 μm. Groups A and B produced similar lineshapes, which were also similar to the sound enamel control lineshape, but differences were observed. First, group A and B specimens produced scattering that recovered around 36 μm and 48 μm, respectively. Second, group B specimens produced greater scatter intensity relative to Group A specimens; in fact, group B produced the largest scattering signal among the five groups. Statistical considerations were made only with respect to the two fluoride dentifrice groups in order to compare these present results with previous micro-computed tomography results [12,13]. Between the two fluoride dentifrice groups, significant differences were found ($p < 0.05$) with group B significantly greater than group A at the 12, 18, 114 and 120 μm measurement increments.

The mean normalized integrated intensity of the equatorial small-angle X-ray scattering from the surface of enamel down to 150 μm in 6 μm increments is shown in Figure 13. The total equatorial intensity was obtained by summing the intensity in the region $q > 1.1$ nm^{-1}. Normalization was similarly performed as discussed above [7,8]. Relative to the sound enamel control, intensity profiles were distinct among groups. The intensity from WSL control specimens produced a unique lineshape that peaked near 36 μm and trailed beyond 100 μm. Group C produced a similar lineshape and maximum intensity at 36 μm compared to the WSL control but recovered near 84 μm. Group A specimens produced a narrower lineshape relative to group C and WSL specimens, peaking around 30 μm and recovering near 72 μm. Group B specimens produced the strongest intensity, peaking at 24 μm and recovering near 72 μm. Statistical considerations were again made only with respect to the two fluoride dentifrice groups in order to compare these present results with previous micro-computed tomography results [12,13]. Between the two fluoride dentifrice groups, significant differences were found ($p < 0.05$) with group B significantly greater than group A at the 0, 12, 18, 24, 30, 36 and 42 μm measurement increments.

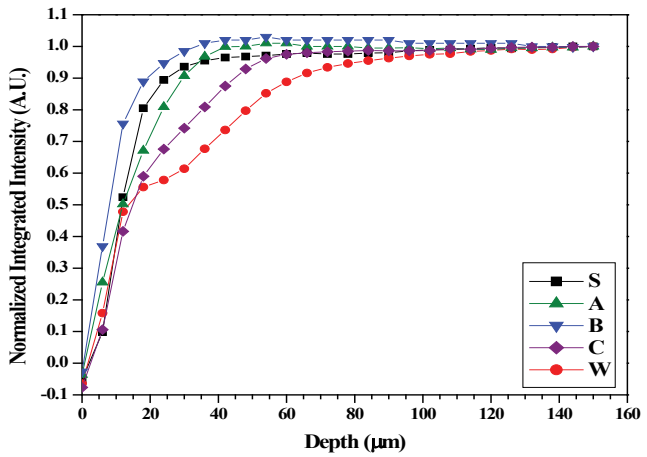

Figure 12: The mean normalized integrated intensity of the equatorial (100) HAp reflection from the surface of enamel down to 150 μm within the enamel cross-section. The letters correspond to the following groups: 0.21% NaF dentifrice (**A**); 1.1% NaF dentifrice (**B**); 0% NaF dentifrice (**C**); sound enamel control (**S**); and, WSL control (**W**).

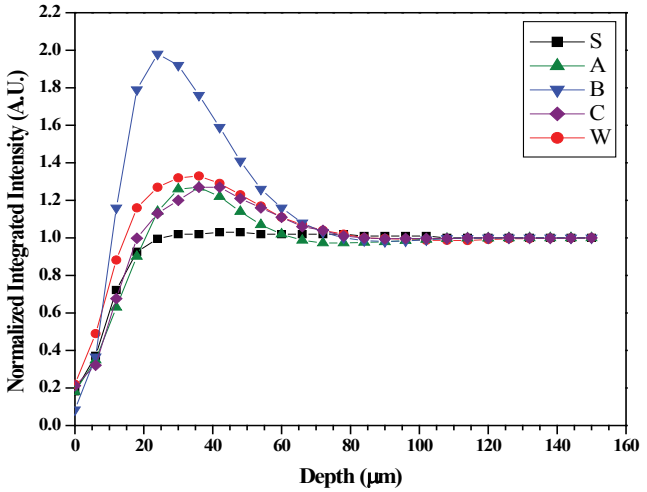

Figure 13: The mean normalized integrated intensity of the equatorial small-angle X-ray scattering from the surface of enamel down to 150 μm within the enamel cross-section. The letters correspond to the following groups: 0.21% NaF dentifrice (**A**); 1.1% NaF dentifrice (**B**); 0% NaF dentifrice (**C**); sound enamel control (**S**); and, WSL control (**W**).

Discussion

Nearly 55 years ago a breakthrough was published on the ability to measure the strengthening effect of calcium and phosphate on demineralized enamel [30]. Realizing calcium-deficient mineral zones are manifest in dental apatite [14,15], topical therapies (e.g. fluoride dentifrice) are a widely used frontline approach in preventing, arresting or even reversing the caries process [31]. An especially clinically effective option, 1.1% NaF dentifrices are designed for those most at-risk for caries development, including those with a history of caries [23,32]. Additionally, modalities manifesting a combination of fluoride (e.g. between 900 and 1450 ppm F^-) and other agents, including various forms of calcium and phosphate, are driving innovations in topical therapies and raising the bar on the level of standard care [2]. Concomitant with such endeavors, advances in experimental techniques continue to provide new tools in order to learn more about the caries process [7,9], including the influence of topical fluorides on enamel lesion microstructure.

The aim of the present study was to assess the microstructure of incipient caries lesions treated with 0.21% and 1.1% NaF dentifrices *in vitro*. This is the first report on the application of WAXD/SAXS measurements on incipient enamel lesions subject to a pH cycling model comprising dentifrice treatments acid challenge and remineralization events. The *in vitro* pH cycling model and the incipient enamel lesions used in this study were chosen based on their established sensitivity to fluoride and clinical relevance [6,19-23]. The two fluoride dentifrices (Clinpro Tooth Crème and Clinpro 5000) comprise a functionalized tricalcium phosphate component that is designed to complement and improve fluoride's mineralizing action on weakened enamel [6,21,33,34]. Also, these dentifrices have demonstrated clinical efficacy and are available in many countries throughout the world [23,35-39]. As the inactive ingredient composition and dentifrice format are nearly similar between the two dentifrices (with the primary exception of fluoride content), these dentifrices provide a unique opportunity to test the fluoride dose-response effect on lesion microstructure without the influence of dentifrice formulation factors (e.g. abrasive system, fluoride salt, foaming characteristics, viscosity, pH, etc.).

With respect to sound and WSL enamel, it is known that surviving crystallites in carious enamel tend to be wider and thicker compared to sound enamel [15], and this is consistent with our FE-SEM results. CSMH measurements correlate with mineral content as shown in transverse microradiography of enamel lesions [24,25]. Though larger crystals may exist in the WSL, the frank reduction in the volume of crystals upon lesion formation is clear based on our CSMH and WAXD results. Also, the mixed orientation of crystallites generated upon lesion formation, as shown in our FE-SEM results, may contribute to the relatively weak enamel microstructure. The sharply resolved but diminutive scatter signal

in the SAXS pattern for sound enamel, suggests it arises from non-mineral material, such as carbonate and water, residing in the inter-crystallite spacings [7]. This signal appears more pronounced in the SAXS pattern for WSL enamel, and can be attributed to the surface scattering encompassing voids that evolved due to dissolution of crystallites during lesion formation [7,15]. Overlapping this oriented feature, the relatively intense smear-like scatter pattern from the WSL control specimen suggests the lesion formation process produced substantial crystallite dissolution along all three crystal axes, including the loss of entire crystallites. Based on ultrastructural studies of carious lesion formation in apatite, the dissolution of enamel during lesion formation likely initiates along the (100) HAp plane where defects (e.g. edge dislocations, screw dislocations, small angle boundaries, atomic vacancies or rotations) in the imperfect enamel abound [14-18]. The nearly concomitant recoveries of the WAXD and SAXS intensities around 100 μm in the WSL enamel indicate the incipient lesions formed in this study do not effect marked structural changes within the deeper sound enamel regions, and contrasts with a previous report that utilized larger subsurface lesions [7].

Remineralization of the subsurface lesions by the three dentifrice groups likely transpired by several mechanisms, including restoration of partially dissolved crystals, the formation of new crystals, and the growth of surviving crystals manifest in the carious lesion [15]. All three dentifrice groups will almost certainly undergo growth of surviving crystals by virtue of the pH cycling model, which was designed to favor remineralization. The SAXS measurements may include information related to restoration of partially dissolved crystals as well as new crystal formation.

The fluoride-free dentifrice group (Tom's of Maine) effected remineralization that led to an increase in CSMH and WAXD intensity. FE-SEM results indicate the mineralization effect produces apatite-like crystallites; however, the crystallites seem to lack regularity in size and orientation. This fluoride-free group relied primarily on the artificial saliva to both nucleate and grow mineral within the incipient lesions, and is similar to results demonstrating the remineralization effect of artificial saliva [8]. Among the three dentifrice groups the fluoride-free group produced the weakest CSMH over the 10-day cycling protocol, indicating the artificial saliva constituents were not able to generate strong, acid-resistant mineral in the course of repeated acidic exposures. The observation that the fluoride-free dentifrice group produced a similar CSMH slope compared to the control WSL within the subsurface region (i.e. up to 75 μm) indicates that the existing subsurface microstructure environments remained similar during the cycling protocol. Furthermore, the (100) intensities across enamel depth also displayed similar trending between the fluoride-free and WSL control groups. Importantly, there is the possibility that non-enamel-like calcium phosphate mineral may also have formed within the subsurface region. An example of such mineral might be the metastable hydroxyapatite precursor, octacalcium phosphate (OCP), which bears ultrastructure similarities to hydroxyapatite and has been described as manifesting apatitic layers in its unit cell structure [40]; in fact, the close lattice-matching of OCP with HAp favors the growth of apatite from OCP crystals [40,41]. The slight differences in the SAXS profiles may also provide some distinctions and suggests a modest reduction in voids (relating to void surface area rather than volume) by the fluoride-free group by the evolution of new crystal formation. Such development appears reasonable given the morphology of the mineral as shown by FE-SEM, and when CSMH results are included, these results collectively suggest the formation of new crystalline material strengthened the lesion microstructure relative to the WSL control group.

The 0.21% NaF dentifrice group (Clinpro Tooth Crème), which contains a conventional amount of fluoride recommended for daily use by most populations [31], produced a distinct remineralization profile relative to the other two dentifrice groups. Over the course of the 10-day cycling protocol, this dentifrice increased the volume of apatite crystals and increased the strength of the WSL microstructure. Concomitant with the increase in apatite crystals as shown in the WAXD profile, the SAXS lineshape indicates the 0.21% NaF dentifrice affected void distribution, resulting in a relatively narrower lineshape that recovers near the boundary of the lesion (which is about 75 μm). This SAXS profile appears distinct compared to both the fluoride-free group and the WSL control, and may suggest the formation of new crystals within the body of the incipient lesion. As FE-SEM demonstrated the presence of dense, well-oriented and apatite-like enamel had formed within the subsurface lesion, this remineralization also improved the strength of the lesion microstructure as measured by CSMH. The primary reason for this improved action in the subsurface lesion is due to the presence of the fluoride ion, which has long been shown to increase acid-resistance of enamel [1]. Additionally, when combined with calcium and phosphate in solution, fluoride has been shown to be an excellent nucleator of mineral [42], and may function as a catalyst in the conversion of OCP to apatite [41]. In this instance, the 0.21% NaF dentifrice provided strong, acid-resistance remineralization relative to the fluoride-free group and the WSL control. This dentifrice also contains the functionalized tricalcium phosphate agent (0.05 wt. %), which is designed to extend the action of fluoride and subsequently improve mineralization, especially within subsurface lesions [6,21-23,34].

At content about five times higher than the 0.21% NaF dentifrice, the 1.1% NaF dentifrice group also conferred strong, acid-resistant remineralization activity. A distinctive property of high-fluoride gels and dentifrices is the relatively confined action of fluoride at the enamel surface [23,32]. However, the 1.1% NaF dentifrice evaluated in this study also contains functionalized tricalcium phosphate (0.08 wt. %), which has been shown to extend fluoride's action deeper within the subsurface lesion, without sacrificing fluoride's action at the enamel surface [2,6,23,34,36,37]. But the abundance of fluoride delivered from the dentifrice influences the morphology and composition of newly formed mineral. As shown in the FE-SEM images, the morphology of the mineral within the subsurface lesions demonstrates a dense population of crystallites. The appearance of these crystallites is not the same as those formed with the 0.21% NaF dentifrice, suggesting the thermodynamics of mineral formation favor smaller crystals at higher fluoride content. In addition to the (100) reflection of HAp observed in the WAXD

pattern and normalized intensity plot, there exists possibilities that fluoride could incorporate within existing apatite framework (e.g. isomorphically replacing OH^-) or contribute to newly formed fluorapatite crystals, which manifest a lattice interval (d = 8.12 Å) similar to that of hydroxyapatite (d = 8.17 Å) [15]. Additionally, the possibility of small angle boundary defects from newly formed apatite crystal imperfectly aligned with the existing enamel framework may also contribute to WAXD measurements. It is reasonable that newly formed crystals are a mixture of the above mentioned possibilities, given the complexities of mineralization in subsurface lesions [15]. Of particular interest is the SAXS profile produced by the 1.1% NaF dentifrice, which produced strong scattering intensity within the subsurface region. The SAXS setup used in this study is sensitive to material (or phases) having nanometer-sized dimensions (e.g. between 1 and 100 nm). Because the scattering reflects an environment having a large electron density, the strong scatter intensity may be attributed to an abundance of newly formed nanometer-sized crystallites. This view is supported with the existence of nanometer sized crystallites within the subsurface region as shown in the FE-SEM image. Further investigation into these mechanistic details, as well as other variations of remineralization (or demineralization) experiments are reserved for future studies.

Conclusions

In addition to digital light microscopy, high-resolution field-emission scanning electron microscopy (FE-SEM) and microhardness measurements, we utilized the BL40XU beamline of the SPring-8 third-generation synchrotron radiation facility in Hyogo, Japan to collect WAXD and SAXS data within incipient enamel lesions. This is the first report that utilized the simultaneous WAXD/SAXS technique to explore microstructure of incipient lesions subjected to a remineralization/demineralization protocol involving dentifrice treatments having different levels of fluoride. A main conclusion from this work is that the WAXD and SAXS measurements were able to resolve significant differences between the effects of two fluoride-containing dentifrices on subsurface lesion microstructure. Altogether, our observations demonstrate the pathological processes for remineralization are markedly influenced by the presence and concentration of fluoride, the microstructural characteristics of which can be distinguished using the simultaneous WAXD and SAXS technique.

Acknowledgment

The synchrotron radiation experiments were performed at the BL40XU of SPring-8 with the approval of the Japan Synchrotron Radiation Research Institute (JASRI) (Proposal No. 2014B1048). We thank Mr. Allen C. Mackey for assistance with cross-sectional micro hardness measurements. Dr. Takatsugu Kobayashi advised preparing enamel slabs. Dr. Kenichi Shimizu who is honorary professor at Keio University and visiting professor at Osaka city University advised sample preparation, FE-SEM selection and SE2 and In-lens detector selection.

Author Contributions

Makoto Asaizumi conceived the project, assisted in study design, data collection, data interpretation, and manuscript preparation. Naoto Yagi designed WAXD/SAXS measurement and assisted in X-ray data analyses. Koki Aoyama built the WAXD/SAXS system and assisted in X-ray data analyses. Tomoaki Kato assisted in WAXD/SAXS data collection and analyses. Shinichi Nagase contributed to X-ray analyses, including the development of the VB software. Tetsuya Kuga participated in sample preparation and data collection. Nahoko Oode, Takehide Oda, and Tsuguo Sakurada participated in FE-SEM design and data collection. Tomohiro Tabara assisted in light microscopy design and data collection. Robert Karlinsey assisted in study design, data interpretation and manuscript preparation.

Conflicts of Interest

Dr. Karlinsey is the managing member of Indiana Nanotech, which has a commercial relationship with 3M Oral Care, whose products were used in this manuscript. Miss. Oode, Drs. Asaizumi, Yagi, Kato, Kuga, and Messrs. Aoyama, Oda, Sakurada, Nagase and Tabara declare no conflicts of interest.

References

1. Muhler JC, Radike AW, Nebergall WH, Day HG. The effect of a stannous fluoride-containing dentifrice on caries reduction in children (1954) J Dent Res 33: 606-612.
2. Amaechi BT. Remineralization therapies for initial caries lesions (2015) Current Oral Health Reports 2: 95-101.
3. Featherstone JD, Doméjean S. The role of remineralizing and anticaries agents in caries management (2012) Adv Dent Res 24: 28-31.
4. Sullivan HR. The formation of early carious lesions in dental enamel. I (1954) J Dent Res 33: 218-230.
5. White DJ. The comparative sensitivity of intra-oral, in vitro, and animal models in the 'profile' evaluation of topical fluorides (1992) J Dent Res 71 Spec No: 884-894.
6. Karlinsey RL, Mackey AC, Walker ER, Amaechi BT, Karthikeyan R, et al., Remineralization potential of 5,000 ppm fluoride dentifrices evaluated in a pH cycling model (2010) J Dent Oral Hygiene 2:1-6.
7. Yagi N, Ohta N, Matsuo T, Tanaka T, Terada Y, et al.. Evaluation of enamel crystallites in subsurface lesion by microbeam X-ray diffraction (2009) J Synchrotron Radiat 16: 398-404.
8. Tanaka T, Yagi N, Ohta T, Matsuo Y, et al., Evaluation of the distribution and orientation of remineralized enamel crystallites in subsurface lesions by X-ray diffraction (2010) Caries Res 44: 253-259.
9. Gaiser S, Deyhle H, Bunk O, White SN, Müller B. Understanding nano-anatomy of healthy and carious human teeth: a prerequisite for nanodentistry (2012) Biointerphases 7: 4.
10. Deyhle H, White SN, Bunk O, Beckmann F, Müller B. Nanostructure of carious tooth enamel lesion (2014) Acta Biomater 10: 355-364.
11. Siddiqui S, Anderson P, Al-Jawad M. Recovery of crystallographic texture in remineralized dental enamel (2014) PLoS One 9: e108879.
12. Asaizumi M, Karlinsey RL, Mackey AC, Kato T, Kuga T. In vitro assessments of white-spot lesions treated with NaF plus tricalcium phosphate (TCP) toothpastes using microtomography (micro-CT) (2013) J Dent Oral Hygiene 5: 68-76.
13. Asaizumi M, Uesugi K, Hoshino M, Kato T, Mackey AC, et al., In vitro assessments of white-spot lesions treated with NaF plus tricalcium phosphate (TCP) toothpastes using synchrotron radiation micro-computed tomography (SR micro-CT) (2014) J Dent Oral Hygiene 6:10-21.
14. Featherstone JD, Goodman P, McLean JD. Electron miscroscope study of defect zones in dental enamel (1979) J Ultrastruct Res 67: 117-123.
15. Yanagisawa T, Miake Y. High-resolution electron microscopy of enamel-crystal demineralization and remineralization in carious lesions (2003) J Electron Microsc (Tokyo) 52: 605-613.
16. Voegel JC, Frank RM. Stages in the dissolution of human enamel crystals in dental caries (1977) Calcif Tissue Res 24: 19-27.
17. Arends J, Jongebloed WL. Ultrastructural studies of synthetic apatite crystals (1979) J Dent Res 58: 837-843.
18. Kerebel B, Daculsi G, Kerebel LM. Ultrastructural studies of enamel crystallites (1979) J Dent Res 58: 844-851.
19. White DJ. Reactivity of fluoride dentifrices with artificial caries. I. Effects on early lesions: F uptake, surface hardening and remineralization (1987) Caries Res 21: 126-140.

20. White DJ. Use of synthetic polymer gels for artificial carious lesion preparation (1987) Caries Res 21: 228-242.

21. Karlinsey RL, Mackey AC, Walker ER, Frederick KE. Surfactant-modified ß-TCP: structure, properties, and in vitro remineralization of subsurface enamel lesions (2010) J Mater Sci Mater Med 21: 2009-2020.

22. Mensinkai PK, Ccahuana-Vasquez RA, Chedjieu I, Amaechi BT, Mackey AC, et al.. In situ remineralization of white-spot enamel lesions by 500 and 1,100 ppm F dentifrices (2012) Clin Oral Investig 16: 1007-1014.

23. Amaechi BT, Ramalingam K, Mensinkai PK, Chedjieu I. In situ remineralization of early caries by a new high-fluoride dentifrice (2012) Gen Dent 60: e186-192.

24. Featherstone JD, ten Cate JM, Shariati M, Arends J. Comparison of artificial caries-like lesions by quantitative microradiography and microhardness profiles (1983) Caries Res 17: 385-391.

25. Kielbassa AM, Wrbas KTh, Schulte-Monting J, Hellwig E. Correlation of transversal microradiography and microhardness on in situ-induced demineralization in irradiated and nonirradiated human dental enamel (1999) Arch Oral Biol 44: 243-251.

26. Inoue K, Oka T, Suzuki T, Yagi N, Takeshita K, et al., Present status of high flux beamline (BL40XU) at Spring-8 (2001) Nuclear Instruments and Methods A467-468: 674-677.

27. Ohta N, Oka T, Inoue K, Yagi N, Kato S, et al., Structural analysis of cell membrane complex of a hair fibre by micro-beam X-ray diffraction (2005) J Appl Cryst 38: 274-279.

28. Peng Z, Gong J, Miao H. On the description of indentation size effect in hardness testing for ceramics: Analysis of the nanoindentation data (2004) J Eur Ceram Soc 24: 2193-2201.

29. Xu C, Reed R, Gorski JP, Wang Y, Walker MP. The Distribution of Carbonate in Enamel and its Correlation with Structure and Mechanical Properties (2012) J Mater Sci 47: 8035-8043.

30. Koulourides T, Cueto H, Pigman W. Rehardening of softened enamel surfaces of human teeth by solutions of calcium phosphates (1961) Nature 189: 226-227.

31. Walsh T, Worthington HV, Glenny AM, Appelbe P, Marinho VCC, et al. Fluoride toothpastes of different concentrations for preventing dental caries in children and adolescents (2010) Cochrane Database Syst Rev 1: CD0076868.

32. Tavss EA, Mellberg JR, Joziak M, Gambogi RJ, Fisher SW. Relationship between dentifrice fluoride concentration and clinical caries reduction (2003) Am J Dent 16: 369-374.

33. Karlinsey RL, Mackey AC, Walker ER, Frederick KE. Preparation, characterization and in vitro efficacy of an acid-modified beta-TCP material for dental hard-tissue remineralization (2010) Acta Biomater 6: 969-978.

34. Karlinsey RL, Pfarrer AM. Fluoride plus functionalized Î²-TCP: a promising combination for robust remineralization (2012) Adv Dent Res 24: 48-52.

35. Vanichvatana S, Auychai P. Efficacy of two calcium phosphate pastes on the remineralization of artificial caries: a randomized controlled double-blind in situ study (2013) Int J Oral Sci 5: 224-228.

36. Mannaa A, Carlén A, Zaura E, Buijs MJ, Bukhary S, et al.. Effects of high-fluoride dentifrice (5,000-ppm) on caries-related plaque and salivary variables (2014) Clin Oral Investig 18: 1419-1426.

37. Mannaa A, Campus G, Carlén A, Lingström P. Caries-risk profile variations after short-term use of 5000 ppm fluoride toothpaste (2014) Acta Odontol Scand 72: 228-234.

38. Naoum SJ, Lenard A, Martin FE, Ellakwa A. Enhancing fluoride mediated dentine sensitivity relief through functionalized tricalcium phosphate activity (2015) International Scholarly Research Notices.

39. Thaper R, Karlinsey RL. Clinical observations on the remineralization of Stage 1 enamel caries lesions using a tray-based protocol: A case report (2015) Int Dent Oral Health 2.

40. Mathew M, Takagi S. Structures of biological minerals in dental research (2001) Journal of Research of the National Institute of Standards and Technology 106: 1035-1044.

41. Iijima M, Nelson DGA, Pan Y, Kreinbrink AT, Adachi M, et al., Fluoride analysis of apatite crystals with a central planar OCP inclusion: Concerning the role of F- ions on apatite/OCP/apatite structure formation (1996) Calcif Tissue Int 59: 377-384.

42. Newesely H. Changes in crystal types of low solubility calcium phosphates in the presence of accompanying ions (1961) Arch Oral Biol 6: 174-180.